Variational Monte Carlo study of the current carried by a quasiparticle

Cody P. Nave,[1] Dmitri A. Ivanov,[2] and Patrick A. Lee[1]
[1]*Department of Physics, Massachusetts Institute of Technology, Cambridge, Massachusetts 02139, USA*
[2]*Institute of Theoretical Physics, École Polytechnique Fédérale de Lausanne (EPFL), CH-1015 Lausanne, Switzerland*
(Received 17 October 2005; revised manuscript received 17 January 2006; published 7 March 2006)

With the use of Gutzwiller-projected variational states, we study the renormalization of the current carried by the quasiparticles in high-temperature superconductors and of the quasiparticle spectral weight. The renormalization coefficients are computed by the variational Monte Carlo technique, under the assumption that quasiparticle excitations may be described by Gutzwiller-projected BCS quasiparticles. We find that the current renormalization coefficient decreases with decreasing doping and tends to zero at zero doping. The quasiparticle spectral weight Z_+ for adding an electron shows an interesting structure in $\mathbf{k}$ space, which corresponds to a depression of the occupation number $n_{\mathbf{k}}$ just outside the Fermi surface. The perturbative corrections to those quantities in the Hubbard model are also discussed.

DOI: 10.1103/PhysRevB.73.104502 PACS number(s): 71.10.−w

I. INTRODUCTION

In recent years, it has been acknowledged that ground-state properties of high-temperature superconductors may be reasonably well-described with the help of Gutzwiller-projected wave functions.[1] However, the main challenge of any candidate theory of high-temperature superconductivity is the description of finite-temperature properties such as the superconducting transition and the pseudogap phenomenon in underdoped cuprates. One of the first issues related to the finite-temperature physics of high-temperature superconductors is the structure of low-lying excitations. Within the framework of Gutzwiller-projected wave functions, the first steps in studying the excitations have been recently made: the quasiparticle spectrum and the quasiparticle spectral weight have been calculated.[2,3] In our paper, we complement the previous studies with the analysis of the current carried by the quasiparticles. The magnitude of the quasiparticle current has a direct physical implication in reducing the superfluid density at finite temperature, which eventually determines the superconducting transition temperature in the underdoped regime.[4,5] Furthermore, the deviation of the quasiparticle current from the prediction of the BCS theory may provide a helpful insight into the physics of high-temperature superconductivity.

The reduction of the superfluid density $n_s(T)/m$ by thermal quasiparticles at the nodes of a d-wave superconductor has been computed by Lee and Wen[4,5] as

$$\frac{\hbar^2 n_s(T)}{m} = \frac{\hbar^2 n_s(0)}{m} - \frac{2\ln 2}{\pi}\alpha^2\left(\frac{v_F}{v_\Delta}\right)k_B T, \tag{1}$$

where v_F and v_Δ are the velocity of the nodal quasiparticles perpendicular and parallel to the underlying Fermi surface, and α is the phenomenological Landau parameter[6] which renormalizes the current carried by the quasiparticle

$$\mathbf{j}(\mathbf{k}) = -e\alpha\mathbf{v}_F. \tag{2}$$

Experimentally, $n_s(T)/m$ can be related to the London penetration depth λ, and the ratio v_F/v_Δ may be extracted independently from a thermal-conductivity measurement.[7] This makes α an experimentally accessible quantity for a variety of doping values.[8,9]

In the first part of the paper, we focus on computing the current renormalization α for different doping values. We find that it decreases with decreasing doping, and that it is roughly constant along the Fermi surface at all dopings. The contribution of particles and holes to the total quasiparticle current allows us to picture the "effective Fermi surface" where the electron contribution crosses over to the hole contribution. We observe that this "effective Fermi surface" deviates considerably from the original Fermi surface of the unprojected BCS state. This reveals the particle-hole asymmetry produced by the Gutzwiller projection.

In the second part of the paper, we discuss another renormalization parameter: the quasiparticle spectral weight Z_+ for adding an electron. The momentum dependence of Z_+ shows a pocket structure at the diagonal of the Brillouin zone just outside the Fermi surface. We further discuss the relations and bounds on Z_+ in the t–J model, as well as corrections arising from the rotation to the Hubbard model.

For our analysis, we take the minimal two-dimensional model for strongly interacting electrons on a lattice, the Hubbard model. Following the usual procedure (see, e.g., Refs. 2 and 10), we first study the wave function for its strong-coupling limit, the t–J model, and then include the first-order correction in t/U due to the doubly occupied sites. The Hamiltonian for the t–J model for our system is defined on the two-dimensional square lattice by

$$\mathcal{H}_{tJ} = -t\sum_{\langle i,j\rangle,\sigma}(c^\dagger_{i,\sigma}c_{j,\sigma} + \text{H.c.}) + J\sum_{\langle i,j\rangle}(\mathbf{S}_i\cdot\mathbf{S}_j - n_i n_j/4), \tag{3}$$

with $t/J=3$. Here $c^\dagger_{i,\sigma}$ is the electron creation operator at site i with spin $\sigma=(\uparrow,\downarrow)$. The $\langle i,j\rangle$ indicates nearest neighbors, $\mathbf{S}_i=\frac{1}{2}c^\dagger_{i,\alpha}\vec{\sigma}_{\alpha,\beta}c_{i,\beta}$, and $n_i=c^\dagger_{i,\alpha}c_{i,\alpha}$. The Hamiltonian (3) is then supplemented with the constraint that no double occupancy is allowed.

We use the variational Monte Carlo technique to calculate expectation values of operators given our trial wave

functions.[11,12] For the t–J model, we consider two related trial wave functions: the ground state wave function $|\Psi_{GS}\rangle$ and the wave function for the excited state $|\Psi_{EX}\rangle$. For the ground state, we use the Gutzwiller-projected d-wave singlet,

$$|\Psi_{GS}\rangle = P_D P_N |\Psi_{BCS}\rangle, \tag{4}$$

where $P_D = \Pi_i [1 - n_{i,\uparrow} n_{i,\downarrow}]$ is the Gutzwiller projection operator onto the subspace with no doubly occupied states, and P_N is the projection operator onto the subspace with N particles. $|\Psi_{BCS}\rangle = \Pi_{\mathbf{k}} [1 + a_{\mathbf{k}} c^{\dagger}_{\mathbf{k},\uparrow} c^{\dagger}_{-\mathbf{k},\downarrow}] |0\rangle$, where $c^{\dagger}_{\mathbf{k},\sigma}$ is the Fourier transform of real-space electron creation operator $c^{\dagger}_{i,\sigma}$. Following the standard BCS definitions for a d-wave singlet state,

$$a_{\mathbf{k}} = \frac{v_{\mathbf{k}}}{u_{\mathbf{k}}} = \frac{\Delta_{\mathbf{k}}}{\xi_{\mathbf{k}} + \sqrt{\xi^2_{\mathbf{k}} + \Delta^2_{\mathbf{k}}}}, \tag{5}$$

$$\Delta_{\mathbf{k}} = \Delta_{var} (\cos k_x - \cos k_y), \tag{6}$$

$$\xi_{\mathbf{k}} = \varepsilon_{\mathbf{k}} - \mu_{var}, \tag{7}$$

with $\varepsilon_{\mathbf{k}} = -2(\cos k_x + \cos k_y)$. Not only has this d-wave Gutzwiller-projected wave function been shown to give good variational energies for the t–J model relative to other possible phases, but also it has correctly reproduced many properties of the superconducting state.[2,13]

For the trial wave function of the low-lying excited states, we take the natural ansatz of the Gutzwiller-projected Bogoliubov quasiparticle[3,14]

$$|\Psi_{EX}(\mathbf{k},\sigma)\rangle = P_D P_N \gamma^{\dagger}_{\mathbf{k},\sigma} |\Psi_{BCS}\rangle. \tag{8}$$

Since the overall normalization of the wave function is of no importance, we may also rewrite the trial excited state as

$$|\Psi_{EX}(\mathbf{k},\sigma)\rangle = P_D P_N c^{\dagger}_{\mathbf{k},\sigma} |\Psi_{BCS}\rangle. \tag{9}$$

Throughout the paper, we suppress the $\mathbf{k}$ and σ variables on $|\Psi_{EX}\rangle$ for notational convenience. The expectation values of any operator O in the variational ground and excited states will be often denoted as $\langle O\rangle_{GS}$ and $\langle O\rangle_{EX}$, respectively.

In our simulations, we use the optimal values of Δ_{var} and μ_{var} calculated for the ground state trial wave function,[15] both for the ground state and for the excited state. These values minimize the expectation value $\langle \mathcal{H}_{tJ}\rangle_{GS}$ of the physical t–J Hamiltonian at a fixed concentration of holes.

We assume boundary conditions that are antiperiodic in the x direction and periodic in the y direction so that we avoid the singularity in $a_{\mathbf{k}}$ along the nodal diagonal, $(0,0)$ to (π,π). A drawback of this choice of boundary conditions is that we are unable to calculate quantities exactly on the nodal diagonal, and instead calculate expectation values for nearby $\mathbf{k}$ points. This becomes an important source of error when we compute expectation values at the nodal point. We try to lower this error by looking at larger systems in order to get better resolution; however, we are limited by our computing resources.

This trial excited state and various related ones have been studied previously by other groups.[3,16–18] The energy dispersion of the low-energy quasiparticles has been found to be of the BCS type $E(\mathbf{k}) = [\xi^2 + \Delta^2_{\mathbf{k}}]^{1/2}$, but with renormalized values of the gap and bandwidth. The nodal point obviously coincides with the nodal point of the unprojected wave function Ψ_{BCS} and slowly shifts inwards from $(\pi/2, \pi/2)$ along the diagonal of the Brillouin zone as the hole doping increases.

II. CURRENT CARRIED BY THE QUASIPARTICLES

In this section, we investigate the current carried by quasiparticles as a function of their momenta and doping. The current carried by the excited state $|\Psi_{EX}(\mathbf{k},\sigma)\rangle$ is defined as

$$\langle \mathbf{j}_{\mathbf{k},\sigma}\rangle = \left\langle \sum_{\langle ij\rangle,\alpha} it(c^{\dagger}_{\alpha,i} c_{\alpha,j} - c^{\dagger}_{\alpha,j} c_{\alpha,i}) \right\rangle^{EX}, \tag{10}$$

where $\langle ij\rangle$ represents a sum over all links. Note that the orientation and direction of the link determines its contribution to the vector $\mathbf{j}$. We can interpret the excited state trial wave function as the ground state for a system of N particles to which we add one unpaired electron so that our state has a net spin and charge. The Gutzwiller projection enforces strong correlation between the added electron and the N-electron ground state, so that we expect an effective quasiparticle with renormalized parameters.

In the standard BCS theory (without the Gutzwiller projection), the current carried by the quasiparticles is $\mathbf{j}_{\mathbf{k}} = e\mathbf{v}_{\mathbf{k}}$ where $\mathbf{v}_{\mathbf{k}} = d\varepsilon_{\mathbf{k}}/d\mathbf{k}$ is the velocity from the underlying normal state and not the velocity from the quasiparticle dispersion $dE/d\mathbf{k}$. This is the result of the fact that in BCS theory the excitations are a superposition of particle and hole states and that these states carry opposite charge but also move in opposite directions. The underlying metallic state can have some Fermi liquid correction to the current carried by the particles and holes. This correction is then carried through to the quasiparticle current in the superconducting state, $\mathbf{j}_{\mathbf{k}} = \alpha e \mathbf{v}_{\mathbf{k}}$. In the case of the Gutzwiller projected trial excited state that we are studying, we see that current does still approximately follow the shape of the dispersion of the underlying metal and that the quasiparticle current renormalization α can be calculated from the ratio of $\mathbf{j}/\mathbf{v}_{\mathbf{k}}$.

A. Current as a function of k

First we examine $\mathbf{j}$, the current carried by the quasiparticle, as a function of $\mathbf{k}$ for various dopings. At most dopings, we find a distribution with a structure similar to what one would expect from the tight binding model. In the top plot of Fig. 1, a typical example of the current carried by the quasiparticle as a function of wave vector is plotted. We compare the direction of the current as a function of momentum to both the quasiparticle dispersion, $dE(\mathbf{k})/d\mathbf{k}$, and to the underlying dispersion of the normal state $\mathbf{v}_{\mathbf{k}}$. We find that the shape of the current indeed approximately follows the dispersion of the normal state and not the dispersion of the quasiparticles. This is the same as in the BCS theory so the Gutzwiller projection does not change this aspect of the physics.

For intermediate doping values, the magnitude of the current reaches its maximum value near the center of the Brillouin zone, and therefore near the nodal point. However, for

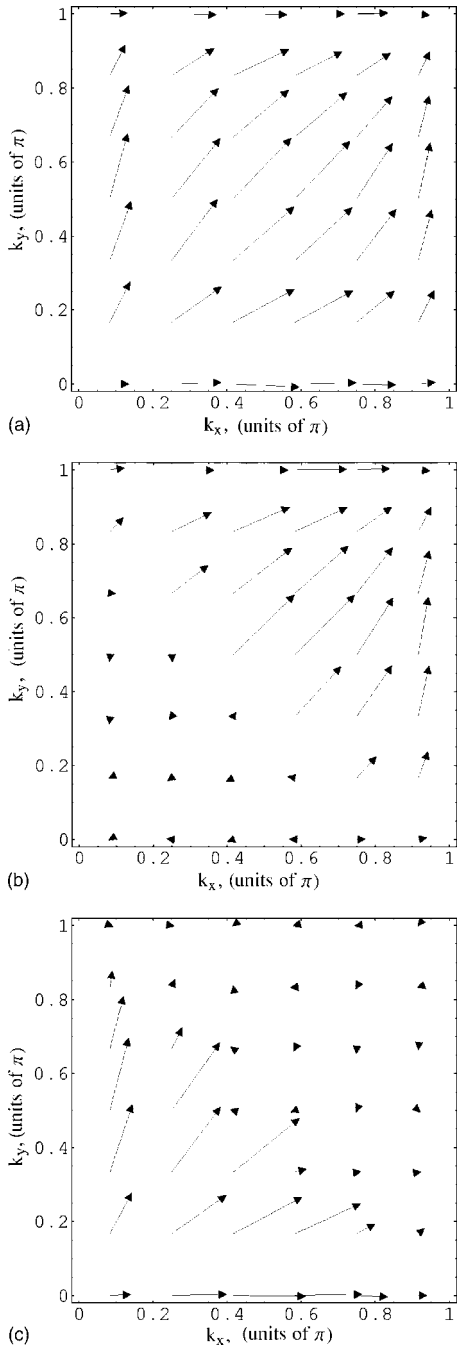

FIG. 1. The top, middle, and bottom figures are, respectively, plots of the current $\mathbf{j}$, $\mathbf{j}_\uparrow$, and $\mathbf{j}_\downarrow$ as a function of the wave vector $\mathbf{k}$ for a 12×12 system with 13 holes, $x=0.09$. The vectors are drawn starting at the $\mathbf{k}$-point at which the current is calculated, their length is proportional to the current magnitude.

strongly underdoped simulations, $x<0.05$, we find that the maximum moves inward along the nodal direction, becoming closer to $(\pi/4,\pi/4)$ as the doping approaches zero (see Fig. 2).

We also look at how much of the total current is being carried by the up spins and down spins individually. By restricting the Σ_α in Eq. (10) so that we consider $\alpha=\uparrow$ and $\alpha=\downarrow$ separately, we can investigate this property of our trial excited state. Since we are now distinguishing between these

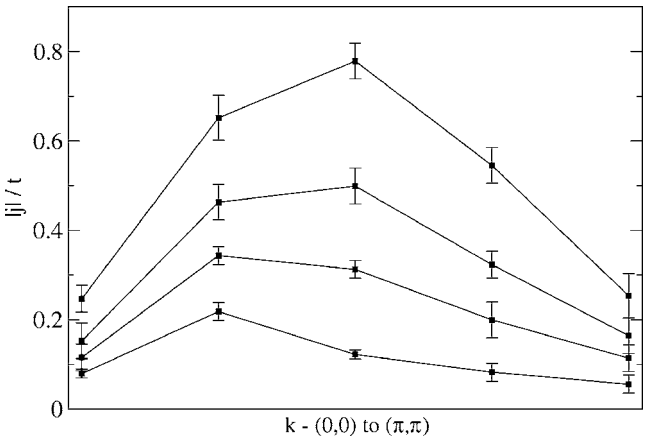

FIG. 2. The magnitude of the current $|\mathbf{j}|$ measured in units of t along the nodal diagonal, $(0,0)$ to (π,π). These runs were done on the 10×10 system with the doping of 0.01, 0.05, 0.09, and 0.17 (increasing magnitude).

two spins, it is important to note that we define our trial wave function as adding an up-spin to the system. Given this, we find that the current of our state is almost entirely carried by either the up spins or the down spins depending on whether or not we are inside or outside of the effective Fermi surface as can be seen in the lower two plots of Fig. 1. Inside of the Fermi surface, all of the current is carried by the down spins and outside of the Fermi surface all of the current is carried by the up spins. This is qualitatively the same as in the unprojected case where the up and down spin currents have factors of $u_\mathbf{k}^2$ and $v_\mathbf{k}^2$, respectively.

To make a more detailed comparison to the BCS theory, we define the "particle contribution" to the current as

$$n_\mathbf{j}=\frac{\mathbf{j}_\downarrow(\mathbf{k})\cdot\mathbf{j}_{\mathrm{tot}}(\mathbf{k})}{|\mathbf{j}_{\mathrm{tot}}(\mathbf{k})|^2}, \tag{11}$$

where $\mathbf{j}_{\mathrm{tot}}=\mathbf{j}_\downarrow+\mathbf{j}_\uparrow$ is the total current carried by the quasiparticle. In the BCS theory, $n_\mathbf{j}(\mathbf{k})=|v_\mathbf{k}|^2$, it takes the values between zero and one, and the isoline $n_\mathbf{j}(\mathbf{k})=0.5$ coincides with the Fermi surface. In Fig. 3 we show the contour plots of $n_\mathbf{j}(\mathbf{k})$ for different values of doping, together with the Fermi surface for the corresponding unprojected BCS wave functions. We see that the "effective Fermi surface" defined by $n_\mathbf{j}(\mathbf{k})$ does not follow the original Fermi surface of the BCS state, but bends outwards in the $(0,\pi)$ regions. Thus it effectively acquires an inward curvature similar to the effect of the negative t' hopping term.

B. Current as a function of doping

We noted earlier that the magnitude of the current has a maximum near the nodal point and that this maximum decreases as a function of doping. In Fig. 4, we plot the magnitude of the nodal current $\mathbf{j}_{\mathrm{nodal}}=\mathbf{j}[\mathbf{k}=(\pi/2,\pi/2)]$ versus doping for both 10×10 and 20×20 systems. Because of our choice of boundary conditions, we do not calculate the current at the true nodal point. For a 10×10 system, the "nodal point" is actually evaluated at $\mathbf{k}=(0.5\pi,0.4\pi)$ and for

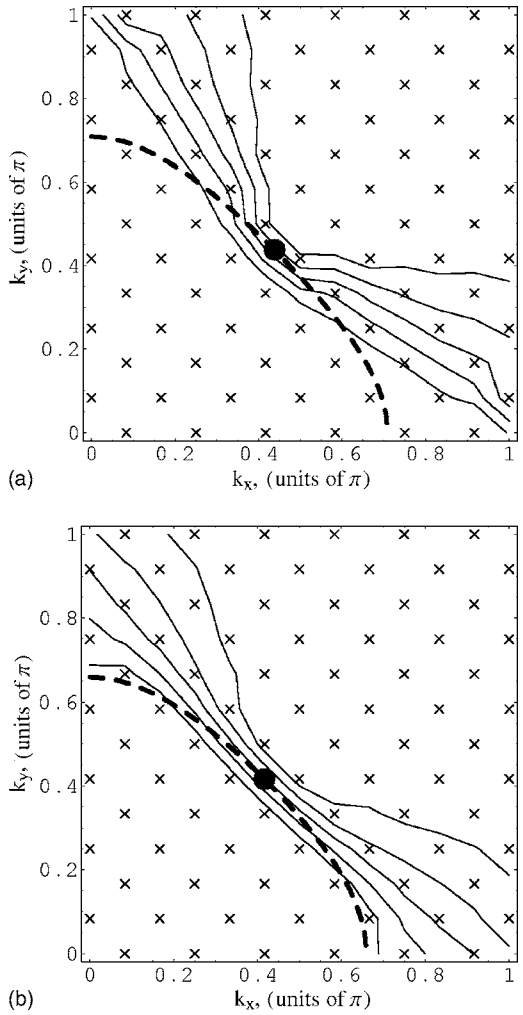

FIG. 3. The particle contribution to the quasiparticle current $n_{\mathbf{j}}(\mathbf{k})$ defined in Eq. (11). The top and the bottom plots correspond to 13 and 31 holes in the 12×12 system (doping $x=0.09$ and $x=0.22$, respectively). The contour lines are $n_{\mathbf{j}}(\mathbf{k})=0.1$, 0.3, 0.5, 0.7, and 0.9 (from left to right). The thick dashed line is the Fermi surface of the unprojected state, the thick solid dot marks the position of the node. Small crosses indicate the positions of data points (we have used the reflection about the x-y diagonal to double the density of data points).

a 20×20 system at $\mathbf{k}=(0.45\pi,0.5\pi)$. In Fig. 4, we see that there is agreement to within the error between the data calculated for two lattices of different size, and we expect that the actual nodal current would also be within these errors.

In the 20×20 system, we can study the doping as low as 0.005 (two holes), and our results indicate that the current apparently decreases down to zero with decreasing doping.

C. Rotation to the Hubbard model

So far we have studied the properties of fully projected wave functions. We would now like to extend our simulations from the t–J model back to the Hubbard model. This can be done in the standard way by employing a unitary transformation e^{iS} that decouples the Hilbert space of the Hubbard Hamiltonian so that there are no matrix elements

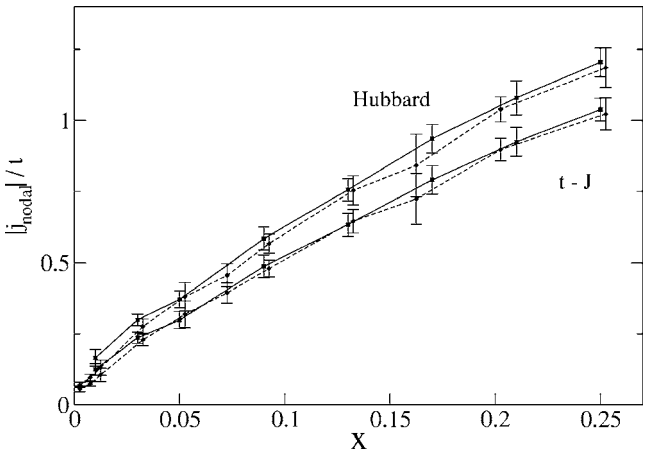

FIG. 4. Magnitude of the nodal current, $|\mathbf{j}_{\text{nodal}}|$ measured in units of t, plotted as a function of doping. The solid lines are the data from a 10×10 lattice and the dashed lines from a 20×20 one. The lower curves are for the trial wave function for the t–J model and the upper curves are for the trial wave function for the Hubbard model (to the lowest order in $t/U=1/12$).

connecting those subspaces with different numbers of doubly occupied sites. Following MacDonald *et al.*,[19] we determine this transformation as a power series in (t/U), so that the subspaces are decoupled order by order. To the first order, the rotation generator is given by

$$iS=\frac{1}{U}(T_1-T_{-1}), \tag{12}$$

where T_1 and T_{-1} are defined to be the parts of the kinetic energy operator that increase and decrease, respectively, the number of doubly occupied sites by one.

With the use of this rotation, we can replace computing the expectation value of any operator O in the ground state of a Hubbard model by computing the expectation value of the rotated operator $\langle e^{iS}Oe^{-iS}\rangle$ in the ground state of the t–J model. We use the same variational wave function for the t–J model as described above and compute the lowest-order correction (linear in t/U) to the t–J expectation value. This procedure has been applied, for example, in the work of Paramekanti *et al.*[10] for calculating the expectation value of the occupation-number operator.

We compute the rotation correction to the value of the nodal current and find that it does not qualitatively change its doping dependence. The corrected value of the current is plotted as the upper curves in Fig. 4 (for $t/U=1/12$).

D. Quasiparticle current renormalization α

Beyond just studying the current itself, we are particularly interested in the quasiparticle current renormalization factor α. As we noted earlier the current and the slope of the dispersion are collinear within the error of our simulations, so we can define $\alpha=\mathbf{j}/\mathbf{v}_{\mathbf{k}}$.

We look at the quasiparticle current renormalization parameter α as a function of doping. We are interested in α for the lowest lying excitations, i.e., for those at the nodal point.

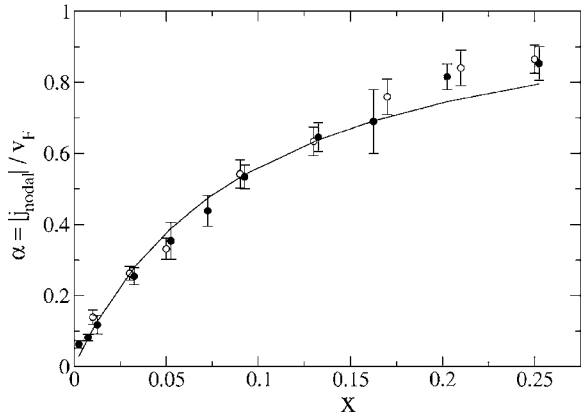

FIG. 5. The renormalization of the quasiparticle current $\alpha=|\mathbf{j}_{\text{nodal}}|/v_F$ as a function of doping. The open circles are for runs on a 10×10 lattice and the closed ones are for runs on a 20×20 one. The solid line is the fit to the 20×20 data by Eq. (16) at $x^*=0.09$.

Although we have calculated the Fermi velocity at the nodal point, more precise data for this velocity as a function of doping are available from the work by Yunoki *et al.*[3] We use those Fermi velocity data in conjunction with our nodal current results to calculate α at the nodal point.

In Fig. 5, we plot the nodal value of α as a function of doping. We find that α goes to zero at zero doping.

It is interesting to compare our results with the predictions of slave-boson theory. In this theory, the low lying excitations are x bosons which carry charge with an effective hopping matrix element proportional to t and fermions which carry spin with an effecting hopping proportional to J. These excitations are coupled to gauge fluctuations. When the gauge fluctuations are treated at the Gaussian level, we obtain the Ioffe-Larkin composition rule which states that the inverse of the superfluid density $\rho_s=n_s/m$ is given by adding the inverses of the fermion and boson contributions:

$$\rho_s^{-1} = (\rho_s^F)^{-1} + (\rho_s^B)^{-1}, \tag{13}$$

where $\rho_s^B \approx xt$ and $\rho_s^F \approx J(1-aT)$ with $a \approx \Delta^{-1}$.[20] Note that the linear temperature dependence comes from thermal excitations of the nodal fermions. Expanding Eq. (13) at small T, we obtain

$$\rho_s(T) \approx \rho_s(0) - \frac{[\rho_s(0)]^2}{\rho_s^F(0)} aT. \tag{14}$$

On the other hand, the quasiparticle dispersion is given by that of the fermions and we can identify v_F/v_Δ in Eq. (1) as being proportional to $aJ \sim a\rho_s^F(0)$. Comparison of Eq. (14) with Eq. (1) results in the simple expression

$$\alpha \sim \frac{\rho_s(0)}{\rho_s^F(0)}, \tag{15}$$

in particular $\alpha \propto x(t/J)$ for $xt < J$.[21] We did not keep track of the numerical coefficients. If we assume that at full doping ($x=1$) α should approach one (the BCS value), Eq. (15) suggests the form

$$\alpha(x) = \frac{x}{x+x^*}(1+x^*), \tag{16}$$

which for $x^*=0.09$ produces a qualitatively good fit of our results for α (see Fig. 5). Note that the order-of-magnitude estimates above give $x^* \sim J/t$, and our best-fit value of x^* is several times smaller.

The shape and the magnitude of the current renormalization parameter α as a function of doping is currently a topic of much experimental work. While there still remain large uncertainties in the experimental data, two useful comparisons can be made to our work. In Ref. 7, the measurements of thermal conductivity and of the penetration depth were used to determine the ratio v_F/v_Δ and the superfluid density. Combining those data resulted in the values of $\alpha=0.66$ and 0.68 for optimally doped samples of BSCCO and YBCO, respectively. Those numbers are in close agreement with our results around $x=0.15$ doping.

Our results also qualitatively agree with the decrease of α as the doping decreases in underdoped YBCO, as reported in Refs. 8 and 9. However, earlier data on YBCO films indicated that the linear T slope of n_s/m is relatively insensitive to doping over a broad range of critical temperatures.[22,23] Since v_F/v_Δ decreases with decreasing x,[24] this trend is in disagreement with Fig. 5 and Eq. (16). It will be desirable to have single crystal data for $n_s(T)/m$ over a broad range of x to settle this point.

On the theoretical side, the recent study of a U(1) slave-boson theory with spinon-holon binding[25] predicted a sublinear dependence of α on the doping. The sublinear form of $\alpha(x)$ disagrees with our proposal (16), but is also consistent with our numerical results shown in Fig. 5.

We further look at α along the Fermi surface for a given doping. We are interested in how the shape and size of this curve changes as a function of doping. While we expect the integral of the whole curve to decrease with x, there are several possibilities for how this could occur. Two such scenarios are that the curve decreases in magnitude everywhere along the Fermi surface uniformly as doping decreases or that α is small almost everywhere along the Fermi surface but that there is a region of large α around the nodal point whose width increases with x. Our numerical results indicate the former of those scenarios. In the upper graph of Fig. 6, we plot the t–J model current magnitude along the Fermi surface. Due to the low finite resolution of our system, we just calculate the current at those points nearest to the line connecting $(\pi,0)$ and $(0,\pi)$. To calculate α, we use the value of v_F found by Yunoki *et al.*[3] along the nodal direction for a given doping and accordingly renormalize the tight binding dispersion to calculate $\mathbf{v_k}$ along these points. We plot α obtained in this way in the lower plot of Fig. 6. We see that α is approximately flat along the Fermi surface.

III. QUASIPARTICLE WEIGHT AND OCCUPATION NUMBER

In this section we examine the quasiparticle weight Z and the occupation number n as a function of momentum and doping. The quasiparticle weight is defined as in Fermi liquid

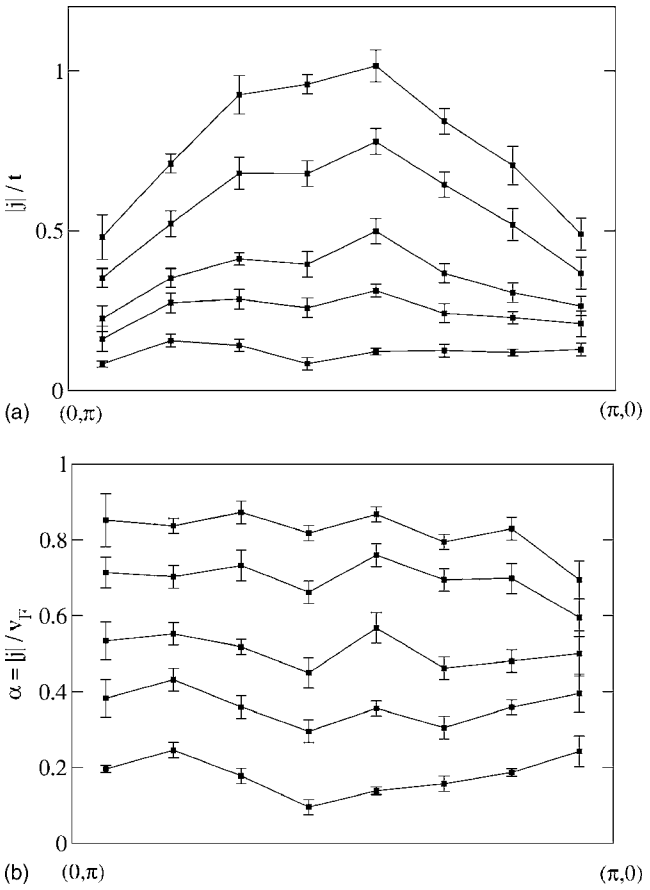

FIG. 6. Plot of $|\mathbf{j}|$ and $\alpha=|\mathbf{j}|/v_F$, upper and lower plots, respectively, for the t–J model along the Fermi surface for dopings of 0.01, 0.05, 0.09, 0.17, and 0.25 (increasing magnitude).

theory and gives a measure of how close our trial wave function quasiparticle is to being a free electron (or a free hole).

We begin with the definitions,

$$Z_+(\mathbf{k},\sigma)=\frac{|\langle\Psi_{\mathrm{EX}}|c^\dagger_{\mathbf{k},\sigma}|\Psi_{\mathrm{GS}}\rangle|^2}{\langle\Psi_{\mathrm{EX}}|\Psi_{\mathrm{EX}}\rangle\langle\Psi_{\mathrm{GS}}|\Psi_{\mathrm{GS}}\rangle}, \tag{17}$$

$$Z_-(\mathbf{k},\sigma)=\frac{|\langle\Psi_{\mathrm{EX}}|c_{\mathbf{k},\sigma}|\Psi_{\mathrm{GS}}\rangle|^2}{\langle\Psi_{\mathrm{EX}}|\Psi_{\mathrm{EX}}\rangle\langle\Psi_{\mathrm{GS}}|\Psi_{\mathrm{GS}}\rangle}, \tag{18}$$

where $|\Psi_{\mathrm{EX}}\rangle$ also carries momentum $\mathbf{k}$, and the electron operators are normalized as $\{c_{\mathbf{k},\sigma},c^\dagger_{\mathbf{k},\sigma}\}=1$. In the BCS theory (without Gutzwiller projection), $Z_+=u^2_{\mathbf{k}}$ and $Z_-=v^2_{\mathbf{k}}$. Along the nodal diagonal (where the gap vanishes), $u^2_{\mathbf{k}}=1$ outside the Fermi surface and 0 inside and $v^2_{\mathbf{k}}$ is the opposite. If one defines $Z=Z_++Z_-$, then in the BCS model $Z=1$ everywhere.

In the projected wave functions, these simple expressions do not apply. However, some of the properties of the spectral weights Z_+ and Z_- may be still proven. Using the identity

$$P_D c^\dagger_k P_D = P_D c^\dagger_k \tag{19}$$

and the d-wave symmetry of the gap, we can prove that along the nodal diagonal,

$$Z_+=0 \quad \text{on} \quad (0,0)-(k_F,k_F), \tag{20}$$

$$Z_-=0 \quad \text{on} \quad (k_F,k_F)-(\pi,\pi), \tag{21}$$

where (k_F,k_F) is the nodal point. Furthermore, Z_+ may be rewritten as the ground-state expectation value

$$Z_+(\mathbf{k},\sigma)=\langle c_{\mathbf{k},\sigma}P_D c^\dagger_{\mathbf{k},\sigma}\rangle_{\mathrm{GS}}. \tag{22}$$

We note that

$$\langle c_{i,\sigma}c^\dagger_{j,\sigma}\rangle_{\mathrm{GS}}=\langle c_{i,\sigma}Pc^\dagger_{j,\sigma}\rangle_{\mathrm{GS}}, \quad i\neq j$$

$$=\langle c_{i,\sigma}Pc^\dagger_{j,\sigma}\rangle_{\mathrm{GS}}+n_{\bar\sigma}, \quad i=j. \tag{23}$$

Thus $Z_+(\mathbf{k},\sigma)$ is further related to the occupation number

$$n_{\mathbf{k},\sigma}=\langle c^\dagger_{\mathbf{k},\sigma}c_{\mathbf{k},\sigma}\rangle \tag{24}$$

as

$$Z_+(\mathbf{k},\sigma)=\frac{1+x}{2}-n_{\mathbf{k},\sigma}. \tag{25}$$

This relation has also been given by Yunoki in Ref. 26. In particular, from this relation follows the upper bound on the spectral weight Z_+:

$$Z_+\leqslant\frac{1+x}{2} \tag{26}$$

and, as a consequence, the same upper bound applies to the nodal spectral weight $Z_{\mathrm{nodal}}=Z_+(k_F+\epsilon,k_F+\epsilon)$ studied by Paramekanti *et al.* in Refs. 2 and 10.

The quasiparticle weight Z_- requires a more complicated Monte Carlo calculation, since it cannot be rewritten as a simple ground-state average like Eq. (22). We therefore restrict ourselves to discussing only the quasiparticle weight Z_+ in this paper.

The above relations for Z_+ have been derived for the fully projected wave function. If we perform a rotation to the Hubbard model, the relations (22) and (25) no longer hold, and the upper bound (26) cannot be proven. Specifically, for the Hubbard model we keep the same definitions of the quasiparticle weights and the occupation number (17), (18), (24), but with the ground and excited states rotated from the fully projected state to the Hubbard-model state by the unitary rotation e^{-iS}, as explained in the previous section. Then the lowest-order Hubbard-model corrections to Z_+ and to $n_{\mathbf{k}}$ may be easily computed as

$$Z^H_+=Z_++2\,\mathrm{Re}\langle c_{\mathbf{k},\sigma}P_D[iS,c^\dagger_{\mathbf{k},\sigma}]\rangle \tag{27}$$

and

$$n^H_{\mathbf{k}}=n_{\mathbf{k}}-2\,\mathrm{Re}\langle c_{\mathbf{k},\sigma}[iS,c^\dagger_{\mathbf{k},\sigma}]\rangle. \tag{28}$$

Even though the two expressions look nearly identical, the correction to $n_{\mathbf{k}}$ does not contain an intermediate projector P_D and, because of that, has a very different structure than that to Z_+. The relation between Z_+ and $n_{\mathbf{k}}$ (25) no longer holds for the Hubbard model, as we shall see below.

Figures 7 and 8 show $Z_+(\mathbf{k})$ for $x=0.03$, 0.12, and 0.21. As noted in Eq. (20), Z_+ is zero along the diagonal between $(0,0)$ and (k_F,k_F) and jumps to a finite value Z_{nodal} at the nodal point. The projected wave function inherits the essen-

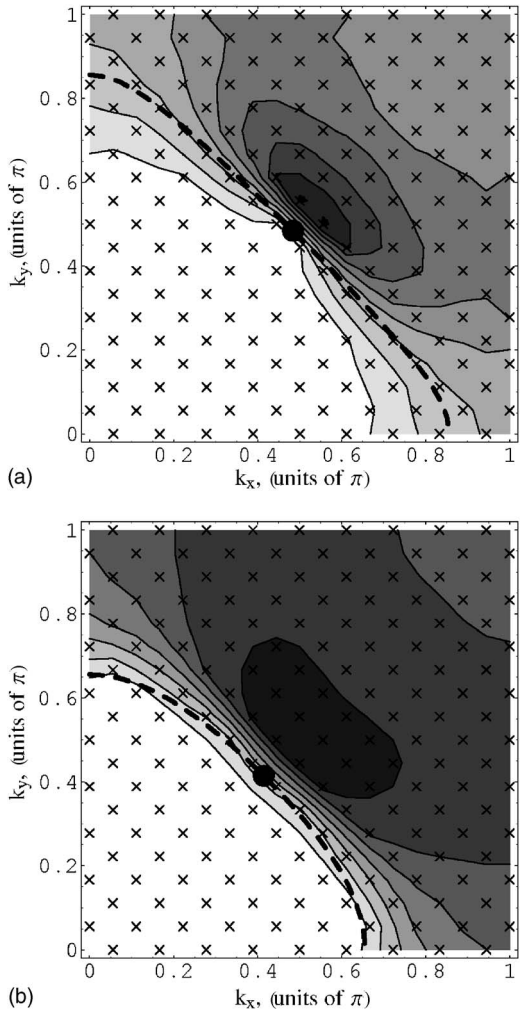

FIG. 7. Contour plots of $Z_+(\mathbf{k})$ in the t–J model for dopings 0.03 (upper plot) and 0.21 (lower plot), 10 and 68 holes in a 18×18 system, respectively. The thick dashed lines denote the Fermi surface of the unprojected wave function, the big solid dot marks the position of the node. Crosses indicate data points used in plotting (available values of the $\mathbf{k}$ vector). In the upper plot, the contour lines correspond to $Z_+=0.01, 0.02, \ldots, 0.09$ (left to right—the maximal value of Z_+ is 0.09). In the lower plot, the contour lines are $Z_+=0.05,0.10,\ldots,0.35$ (with the maximal value $Z_+=0.38$).

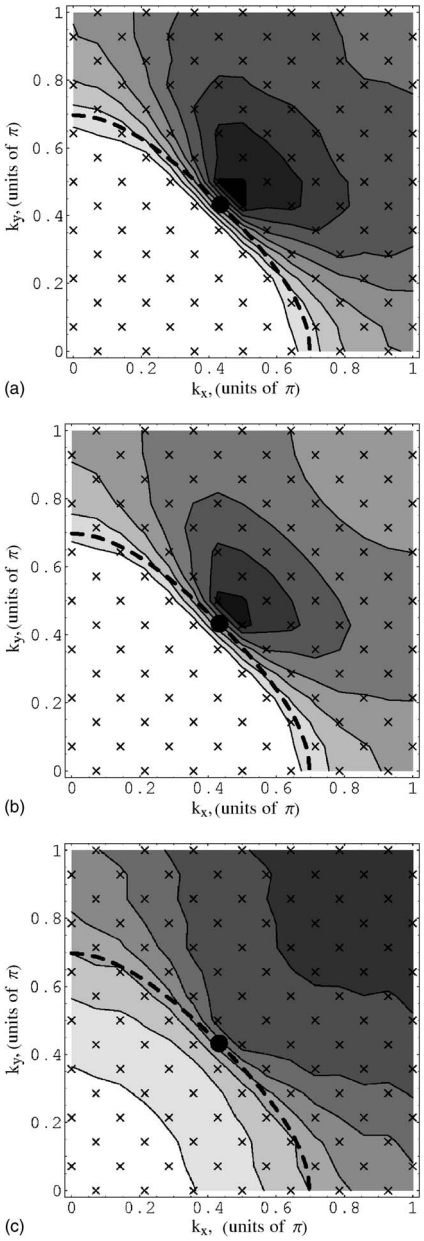

FIG. 8. Upper plot: contour plot of $Z_+(\mathbf{k})$ [or, equivalently, of $n(\mathbf{k})$] in the t–J model at the doping 0.12 (24 holes in the 14×14 system). The isolines correspond to $Z_+=0.03,0.06,\ldots,0.27$ [$n(\mathbf{k})=0.53,0.50,\ldots,0.29$, respectively, left to right]. The maximal value of Z_+ (near the node) is 0.27. Middle plot: Z_+^H in the same system rotated to the Hubbard model (to the first order in $t/U=1/12$), Eq. (27). The isolines correspond to $Z_+^H=0.05,0.10,\ldots,0.35$. The maximal value of Z_+^H (near the node) is 0.37. Bottom plot: $n_{\mathbf{k}}^H$ in the same system rotated to the Hubbard model (to the first order in $t/U=1/12$), Eq. (28). The isolines are $n_{\mathbf{k}}^H=0.8,0.7,\ldots,0.2$ (left to right). The Fermi surface, the nodal point, and the positions of data points are denoted in the same way as in Fig. 7.

tial singularity of Z_+ at the nodal point from the underlying BCS wave function. The value of Z_{nodal} has been studied as a function of doping by Paramekanti *et al.* in Refs. 2 and 10. The doping dependence of Z_{nodal} (Fig. 2 of Ref. 2 and Fig. 6 of Ref. 10) is qualitatively similar to what we find for α (Fig. 5): both Z_{nodal} and α decrease to zero with decreasing doping, with a strong upward curvature. However we are not aware of any *a priori* relation between α and Z_{nodal}.

Using Eq. (25), the plots of $Z_+(\mathbf{k})$ may also be interpreted as those of $n_{\mathbf{k}}$ (see, e.g., the upper plot in Fig. 8). Note the region of depression in $n_{\mathbf{k}}$ just outside the Fermi surface, which resembles a hole "pocket." The existence of this pocket may already be inferred from the nonmonotonous behavior of $n_{\mathbf{k}}$ along the zone diagonal found in Refs. 2 and 10 but the full $\mathbf{k}$ dependence shown in Figs. 7 and 8 gives a more complete picture. Remarkably, a similar "pocket" structure has been found in the U(1) slave-boson model with spinon-holon-binding by Ng.[25] The pocket is more pronounced at lower dopings and appears consistent with the bending of the "effective Fermi surface" defined in Sec. II from $n_{\mathbf{j}}$, Eq. (11). However, to define a meaningful Fermi surface from the quasiparticle spectral weight, one needs an

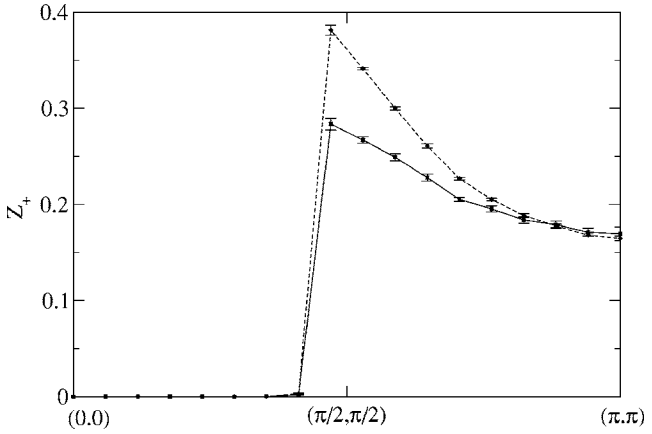

FIG. 9. Plot of Z_+ and Z_+^H, the solid and dashed lines, respectively, for an 18×18 system with 40 holes, $x=0.12$. The data are calculated on the discrete grid points closest to the diagonal.

access also to the spectral weight Z_- which goes beyond the scope of the present paper.

If we include the t/U correction from the rotation to the Hubbard model, the pocket structure in $n_{\mathbf{k}}^H$ disappears, see Fig. 8 (lower plot) and Refs. 2 and 10. On the other hand, including the t/U correction to $Z_+(\mathbf{k})$ preserves the pocket structure, see Fig. 8 (middle plot). This shows that in the Hubbard model the relation (25) between $Z_+^H(\mathbf{k})$ and $n_{\mathbf{k}}^H$ no longer holds.

In Refs. 2 and 10, it was reported that the rotation to the Hubbard model does not change the magnitude of the jump in $n_{\mathbf{k}}$ at the Fermi surface. Our results on $n_{\mathbf{k}}$ and $n_{\mathbf{k}}^H$ confirm this statement, however the spectral weight defined as Z_+ increases when rotated to the Hubbard model. In Fig. 9, we show Z_+ and Z_+^H along the nodal diagonal for an $x=0.12$ system.

IV. CONCLUSION

In this paper, we have analyzed the properties of the excited states in the t–J and Hubbard models in the framework of Gutzwiller-projected variational wave functions. The quantities of main interest are the renormalization of the current and spectral weight of the quasiparticles. Both those renormalizations decrease with decreasing doping and exhibit strongly non-BCS behavior. We also find that the total current is renormalized approximately uniformly along the Fermi surface.

The renormalization of the quasiparticle current allows us to define the effective Fermi surface as a crossover region between the electron- and hole-supported current. We observe that such a Fermi surface bends outwards in the $(0,\pi)$ regions. Such a curvature has been observed in angle-resolved photoemission spectroscopy measurements (see, e.g., Ref. 27 for recent data on LSCO) and is normally ascribed to a negative-t' hopping term. Our observation of an effective renormalization of the Fermi surface by projection suggests another possibility: that the observed holelike shape of the Fermi surface may appear as a result of strong correlations in a t–J (or Hubbard) Hamiltonian with only nearest-neighbor hopping.

We can further see a signature of the Fermi-surface renormalization in the quasiparticle spectral weight $Z_+(\mathbf{k})$. This spectral weight is peaked near the nodal point and exhibits a pocketlike structure with this feature becoming more pronounced at lower doping values. We now assume that $Z=Z_++Z_-$, where Z_+ and Z_- are related to Z as in the BCS case, i.e. $Z_+=Zu_{\mathbf{k}}^2$ and $Z_-=Zv_{\mathbf{k}}^2$. If we now further assume that the total Z is a relatively smooth function of $\mathbf{k}$, then the shape of the pocket is due to the structure of u. Since $u_{\mathbf{k}}^2=\frac{1}{2}(1+\xi_{\mathbf{k}}/E_{\mathbf{k}})$, we see that the shape of u is dependent on the underlying dispersion. The shape of the pocket in Z_+ thus implies a dispersion that has an outward curving Fermi surface. This is consistent with the results from the renormalized current and again points to an origin of this curvature apart from adding t' hopping.

Having looked at the shape of the pocket in Z_+, we now examine its origin. At half-filling the projected staggered-flux (SF) state[15] is identical to the projected d-wave BCS state. Therefore we expect that away from half-filling but still at low dopings that $n(\mathbf{k})$ in the two states will be similar. In the SF state, we know that there are Fermi pockets around $(\pi/2,\pi/2)$, thus we expect some semblance of these pockets in $n(\mathbf{k})$ for the projected d-wave state. Using the relation in the t–J model between n and Z_+, we see that this is consistent with the pocket structure that we found and points to a possible source. We also note that, since the peak falls off smoothly with increasing $|\mathbf{k}|$, it agrees with the proposal of Wen and Lee that the Fermi arc is part of a pocket where the backside arc is unobservable because it has a much lower spectral weight.[5]

Finally, comparing the results for the t–J model and for the Hubbard model (to the lowest order in the t/U correction), we find that the rotation to the Hubbard model does not qualitatively affect the renormalizations of the quasiparticle spectral weight and of the current.

ACKNOWLEDGMENTS

We would like to thank T. K. Lee and C. Castellani for their discussions and help on this research. C.P.N. and P.A.L. acknowledge support by NSF Grant No. DMR-0517222.

[1] P. W. Anderson, P. A. Lee, M. Randeria, T. M. Rice, N. Trivedi, and F. C. Zhang, J. Phys.: Condens. Matter **16**, R755 (2004).

[2] A. Paramekanti, M. Randeria, and N. Trivedi, Phys. Rev. Lett. **87**, 217002 (2001).

[3] S. Yunoki, E. Dagotto, and S. Sorella, Phys. Rev. Lett. **94**, 037001 (2005).

[4] P. A. Lee and X. G. Wen, Phys. Rev. Lett. **78**, 4111 (1997).

[5] X. G. Wen and P. A. Lee, Phys. Rev. Lett. **80**, 2193 (1998).

[6] A. J. Millis, S. M. Girvin, L. B. Ioffe, and A. I. Larkin, J. Phys. Chem. Solids **59**, 1742 (1998).
[7] M. Chiao, R. W. Hill, C. Lupien, L. Taillefer, P. Lambert, R. Gagnon, and P. Fournier, Phys. Rev. B **62**, 3554 (2000).
[8] R. Liang, D. A. Bonn, W. N. Hardy, and D. Broun, Phys. Rev. Lett. **94**, 117001 (2005).
[9] D. Broun, P. Turner, W. A. Huttema, S. Özcan, B. Morgan, R. Liang, W. N. Hardy, and D. A. Bonn, cond-mat/0509223 (unpublished).
[10] A. Paramekanti, M. Randeria, and N. Trivedi, Phys. Rev. B **70**, 054504 (2004).
[11] C. Gros, Ann. Phys. (N.Y.) **189**, 35 (1989).
[12] H. Yokoyama and H. Shiba, J. Phys. Soc. Jpn. **57**, 2482 (1988).
[13] H. Yokoyama and M. Ogata, J. Phys. Soc. Jpn. **65**, 3615 (1996).
[14] P. W. Anderson, Science **235**, 1196 (1987).
[15] D. A. Ivanov and P. A. Lee, Phys. Rev. B **68**, 132501(R) (2003).
[16] T. Giamarchi and C. Lhuillier, Phys. Rev. B **47**, 2775 (1993).
[17] T. K. Lee and C. T. Shih, Phys. Rev. B **55**, 5983 (1997).
[18] W. C. Lee, T. K. Lee, C. M. Ho, and P. W. Leung, Phys. Rev. Lett. **91**, 057001 (2003).
[19] A. H. MacDonald, S. M. Girvin, and D. Yoshioka, Phys. Rev. B **37**, 9753 (1988).
[20] L. B. Ioffe and A. I. Larkin, Phys. Rev. B **39**, 8988 (1989).
[21] P. A. Lee, N. Nagaosa, and X. G. Wen, Rev. Mod. Phys. **78**, 17 (2006).
[22] B. R. Boyce, J. Skinta, and T. Lemberger, Physica C **341-348**, 561 (2000).
[23] J. Stajic, A. Iyengar, K. Levin, B. R. Boyce, and T. R. Lemberger, Phys. Rev. B **68**, 024520 (2003).
[24] M. Sutherland, D. G. Hawthorn, R. W. Hill, F. Ronning, S. Wakimoto, H. Zhang, C. Proust, E. Boaknin, C. Lupien, L. Taillefer, R. Liang, D. A. Bonn, W. N. Hardy, R. Gagnon, N. E. Hussey, T. Kimura, M. Nohara, and H. Takagi, Phys. Rev. B **67**, 174520 (2003).
[25] T.-K. Ng, Phys. Rev. B **71**, 172509 (2005).
[26] S. Yunoki, Phys. Rev. B **72**, 092505(R) (2005).
[27] T. Yoshida, X. J. Zhou, K. Tanaka, W. L. Yang, Z. Hussain, Z.-X. Shen, A. Fujimori, S. Komiya, Y. Ando, H. Eisaki, T. Kakeshita, and S. Uchida, cond-mat/0510608 (unpublished).